Progress In Electromagnetics Research C, Vol. 34, 13–27, 2013

ANALYSIS OF BAND-NOTCHED UWB PRINTED MONOPOLE ANTENNAS USING A NOVEL SEGMENTED STRUCTURE

K. Zhang[1, *], T. Wang[1], and L. L. Cheng[2]

[1]School of Automation, Guangdong University of Technology, Guangdong 510006, China

[2]Faculty of Computer, Guangdong University of Technology, Guangdong 510006, China

Abstract—A novel segmented structure is proposed as a versatile approach to reject certain band of UWB printed monopole antennas (PMAs). To validate the effectiveness of the proposed structure, three UWB PMAs with typical circular, beveled rectangular and regular hexagonal patch shapes are selected and investigated. Good agreement between simulation and measurement shows that, by segmenting every selected patch into three parts, intensive coupling occurs between the center patch and the side patches at the target frequency, and consequently the band-notched function in IEEE 802.11a WLAN band is obtained. The measured radiation properties of these antennas are also presented and discussed. Moreover, a pair of equivalent lumped circuit models is presented, which provides a physical correlation between the notch band behaviors and the control parameters. The input impedance of the antennas calculated by the equivalent circuit models agree very well with the HFSS simulated results.

1. INTRODUCTION

Ultra-wideband (UWB) technologies have attracted considerable attention since the FCC allocated the frequency band of 3.1 GHz to 10.6 GHz for commercial use in 2002. Various types of antennas have been investigated for UWB systems, and among which printed monopole antennas (PMAs) have been widely regarded as an excellent candidate, since they are very compact in size and can be easily integrated with RF circuits and devices [1–4]. However, over the

Received 24 August 2012, Accepted 8 October 2012, Scheduled 24 October 2012

* Corresponding author: Ke Zhang (zhangk@mail2.sysu.edu.cn).

released UWB operation bandwidth, there are some narrow bands occupied by the existing wireless systems such as WLAN operated at $5.15 \sim 5.825\,\mathrm{GHz}$. Therefore, the potential electromagnetic interference (EMI) problems should be paid much attention. Recently, large numbers of band-notched (or say band-rejected) UWB antennas have been investigated and reported, which can reject the certain band within the ultra wide passband without mounting additional bandstop filters [5–17].

Several approaches been proposed to achieve band-notched characteristic. As for PMAs, there are two most conventional approaches: One is to etch various shaped slots or slits in the radiating patch [5, 6], the feedline [7, 8] or the ground plane [9, 10]. Alternative approach is to introduce parasitic elements beside the printed monopole [11–13] or the feedline [14, 15]. It is well known that the ultrawideband properties of PMAs can be attributed to several adjacent resonance modes [16]. Band-notched structure can be regarded as an additional embedded resonance mode which disturbs the inner EM field of the original antenna body at the notched frequency. As a result,the antenna input impedance is shifted to a very high or very low level. From the angle of transmission line model, the antenna here acts as a virtual-open or virtual-short circuit which brings out impedance mismatch at the feed point.

In our previous work, a PMA with a segmented circular patch was presented [17]. In this paper, the segmented structure is studied further in depth as a versatile approach to achieve band-notched characteristic. Two additional UWB PMAs with typical beveled rectangular and regular hexagonal patch shapes are selected and investigated to show the effectiveness of the segmenting approach. The surface current distributions of the proposed antennas are analyzed. All the antennas are carefully optimized, fabricated and measured. The results indicate that, by utilizing the proposed segmented structure, steeper rise in VSWR curve at the notched band is obtained. The center frequency and the bandwidth of the notched band are tunable. The proposed structure could be regarded as a hybrid between the methods of cutting slots and attaching parasitic elements. The parasitic elements (side patches) are generated by segmenting the patch into three parts. It is a simple design compared to other band-notched UWB antennas with parasitic elements [11–13]. Moreover a pair of equivalent lumped circuit models with simple format and high precision is presented which gives physical insight to the proposed band-notched structure and also gives guidance to the parameter optimizations.

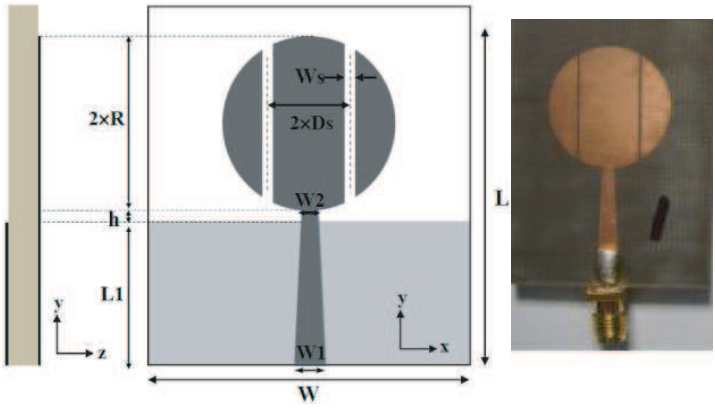

Figure 1. Band-notched UWB antenna with a segmented circular monopole patch (Ant-1).

2. ANTENNA DESIGNS AND RESULTS

According to our previous work, band-notched function of a circular monopole antenna can be obtained by simply segmenting the circular patch with a pair of symmetrical slots, as shown in Figure 1. The center frequency and the bandwidth of the stopband can be adjusted by tuning the position *Ds* and the width *Ws* of the slots. This is based on the fact that, when the position of the slots varies, the slots length and the effective current path along the slots vary accordingly, which leads to the movement of the notched frequency. For UWB PMAs, radiating patches with tapered bottom edges are frequently adopted to broaden the bandwidth. Therefore, it is reasonable to deduce that the segmented structure which brings on band-notched function could be probably applied to other monopole antennas with various patch shapes. In order to validate this point, two additional UWB PMAs with typical patch shapes of beveled rectangle and regular hexagon are selected and investigated, as shown in Figure 2. For simplicity, the segmented circle planar monopole antenna proposed previously in [17] is marked as Ant-1, while the segmented beveled rectangle monopole antenna and the segmented regular hexagon monopole antenna are denoted as Ant-2 and Ant-3 respectively.

As shown in Figure 2, a substrate (WangLing F4Bm-2) with thickness of 1.5 mm, relative permittivity of 3, and dielectric loss angle tangent of 0.0015 is utilized, and a linearly tapered microstrip line is adopted in order to further increase the impedance bandwidth. The tapered microstrip can be regarded as an impedance transformer that

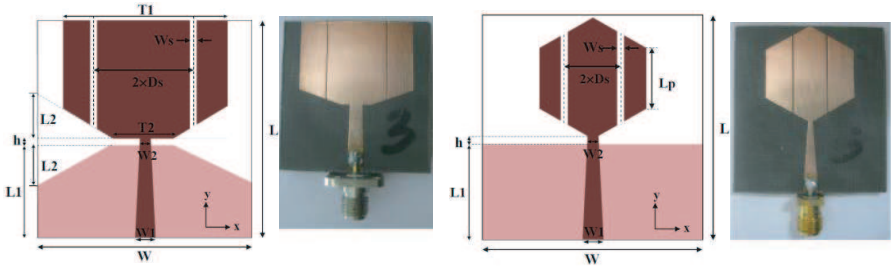

Figure 2. Band-notched UWB antennas with segmented structure placed on (a) beveled rectangle monopole patch (Ant-2) and (b) regular hexagon monopole patch (Ant-3).

smoothly transforms the impedance of the radiating element to 50 Ω of a standard SMA connector [18]. As a result, the bandwidth is enlarged, especially in the high-frequency region.

In design of Ant-2, both the rectangle monopole and the ground plane are beveled. The bottom edge of the patch has the same length with the top edge of the ground plane. A regular hexagonal radiator is adopted in Ant-3. To obtain band notched functions, the proposed segmented structure is implanted into Ant-2 and Ant-3, i.e., cutting apart radiating patches with a pair of symmetrical slots. The side patches function as two parasitic elements and work as bandstop filters. In the notched band, intensive coupling resonance occurs between the center patch and the side patches, which results in low radiation efficiency.

The fullwave electromagnetic simulator Ansoft HFSS is employed to perform the design and optimization. The final geometry parameters for Ant-2 and Ant-3 are as follows.

Ant-2: $L = W = 36\,\text{mm}$, $W1 = 3.8\,\text{mm}$, $W2 = 3\,\text{mm}$, $T1 = 27\,\text{mm}$, $T2 = 7\,\text{mm}$, $L1 = 15\,\text{mm}$, $L2 = 5\,\text{mm}$, $Ds = 3\,\text{mm}$, $Ws = 0.3\,\text{mm}$, $h = 0.6\,\text{mm}$.

Ant3: $L = 43\,\text{mm}$, $W = 38\,\text{mm}$, $W1 = 3.8\,\text{mm}$, $W2 = 0.5\,\text{mm}$, $Lp = 12\,\text{mm}$, $L1 = 18\,\text{mm}$, $Ds = 4\,\text{mm}$, $Ws = 0.3\,\text{mm}$, $h = 1\,\text{mm}$.

Figure 3 shows the HFSS simulated scalar surface current distributions of Ant-2 at radiating frequency 2.35 GHz and notch frequency 5.56 GHz. The 2.35 GHz current mainly distributes along the lower edge of the radiator as well as the feed line. Simultaneously, very little current is observed along the slots, which means the existence of the segmented structure has little effect on the UWB antenna at this frequency. However, at the notch frequency 5.56 GHz, surface

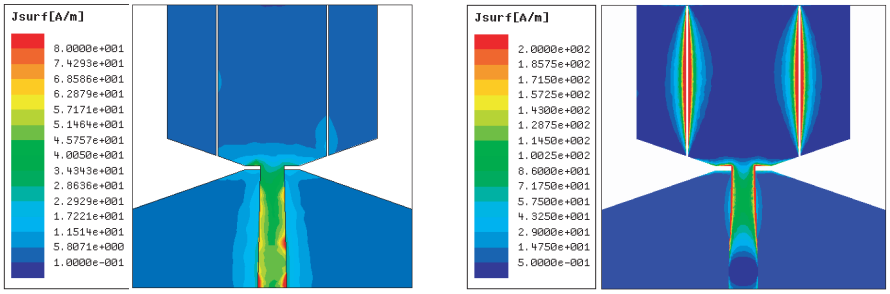

Figure 3. Surface current magnitude distributions of Ant-2 at (a) radiating frequency 2.35 GHz and (b) notch frequency 5.56 GHz.

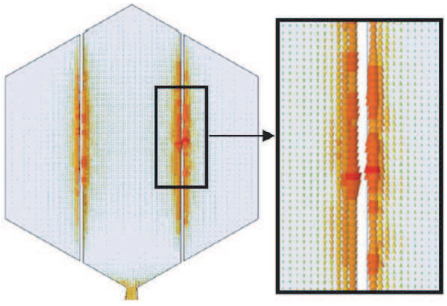

Figure 4. Surface current vector distribution of Ant-3 at notch frequency 5.53 GHz.

current distribution is mainly clustered along the edges of the slots. Similar phenomena are observed in the investigation of Ant-3. Figure 4 shows the vector surface current distributions of Ant-3 at its notch frequency 5.53 GHz. Note that, the current distributions along the edges of the slot are approximately symmetrical but with opposite directions, which causes the antenna to be nonradiative. In such case, the input impedance is singular, making large reflection at the expected frequency.

All the antennas were measured with an Agilent N5241A vector network analyzer, and the results are depicted in Figure 5. For comparison, three un-notched reference antennas without bandnotched structure but with the same configuration and parameter values were also fabricated and measured. As shown in the figure, measured and simulated results track fairly well except a little discrepancy at the low frequency region, which probably dues to the joining of the SMA

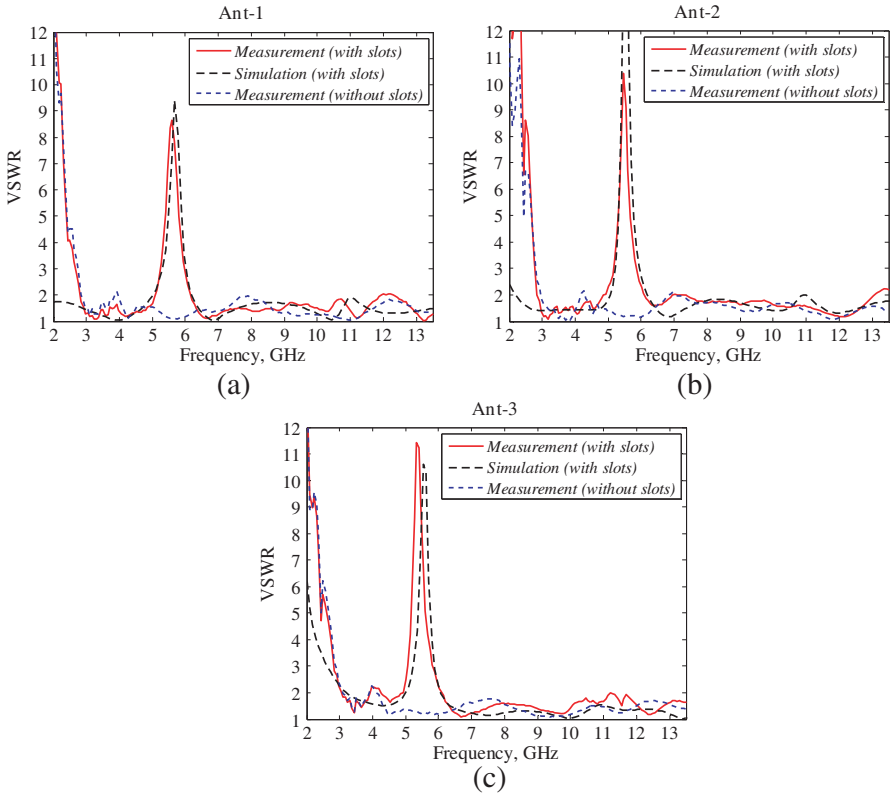

Figure 5. Measured and simulated VSWR values of the proposed band-notched and reference antennas. (a) Ant-1. (b) Ant-2. (c) Ant-3.

connector (solder roughness). The notched band is achieved for all the antennas. The measured stopband of Ant-2 ranges from 4.95 to 5.95 GHz (VSWR > 2) with notch frequency at 5.47 GHz, as shown in Figure 5(b). The measured notch frequency of Ant-3 is 5.25 GHz (5.1–6.1 GHz, VSWR > 2), which is depicted in Figure 5(c). Meanwhile, maximum VSWR above 8 for each antenna is found (8.8, 10.5 and 11.4 for Ant-1$\sim$Ant-3), which means sufficient band-rejection effect is achieved.

Figures 6 and 7 show the measured normalized far-field radiation patterns at different frequencies for Ant-2 and Ant-3 respectively. Note that both antennas are considered to be printed in the xy-plane, where the monopole and the feedline lie along the y-direction, as illustrated in Figure 2. Therefore, the radiation patterns shown in Figures 6 and 7

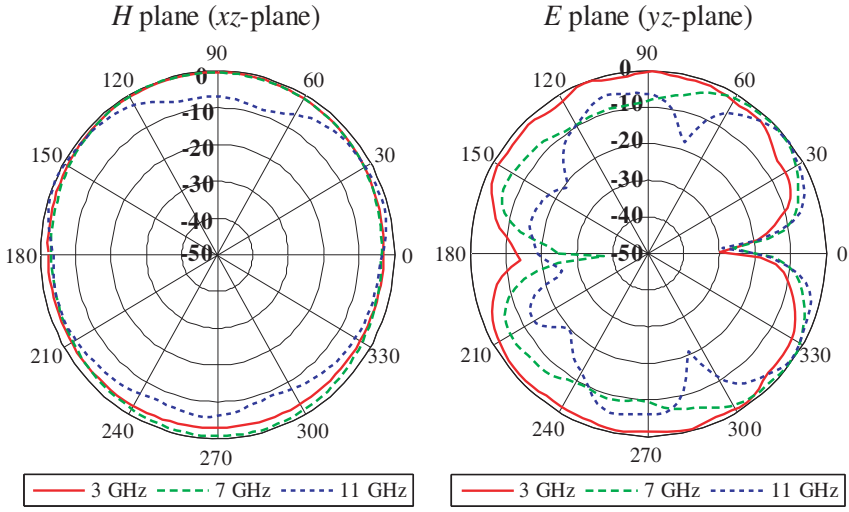

Figure 6. Measured radiation patterns (dB) of Ant-2 on xz plane (H-plane) and yz plane (E-plane), for the 3-, 7-, and 11-GHz frequencies.

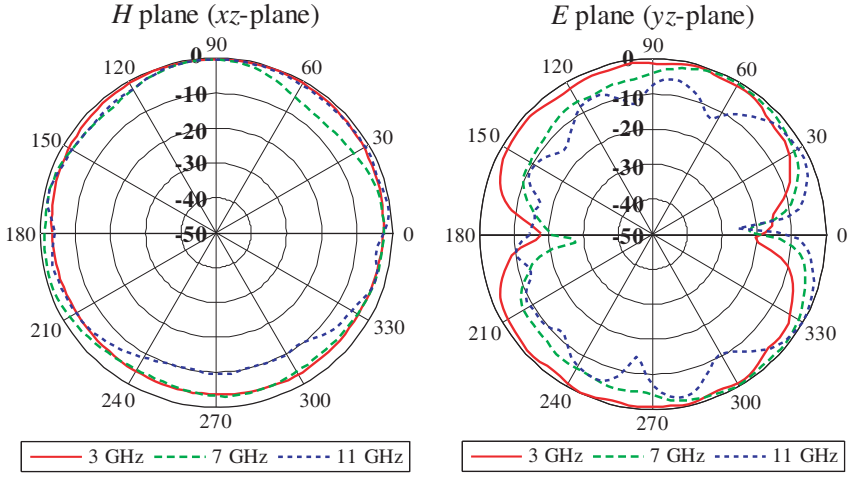

Figure 7. Measured radiation patterns (dB) of Ant-3 on xz plane (H-plane) and yz plane (E-plane), for the 3-, 7-, and 11-GHz frequencies.

are y-polarized without considering the cross polarization. The E-plane is the yz-plane, whereas the H-plane is the xz-plane. As shown in the figures, the H-plane patterns are almost omni-directional for both antennas. In the E-plane, dumbbell shaped radiation patterns

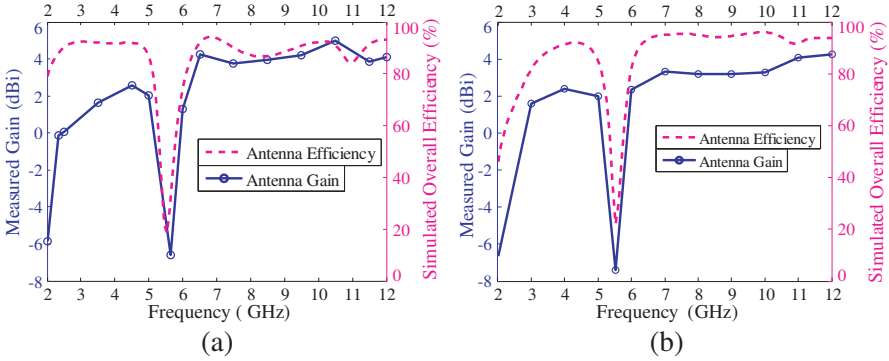

Figure 8. Measured gain and simulated overall efficiency. (a) Ant-2. (b) Ant-3.

are observed at 3 GHz, which is similar to the E-plane patterns of conventional dipole antennas. As frequency increases, the number of the lobes increases because the antennas are no longer small compared to the wavelength. The measurements also indicate that the proposed segmented structure has little impact on the radiation properties of the UWB antennas. Figure 8 illustrates the measured gain and simulated overall efficiency of Ant-2 and Ant-3. For Ant-2, a high rejection (overall efficiency around 20%) is observed at the notch frequency, as shown in Figure 8(a). It indicates that the remarkable gain decrease (-6.73 dBi) at 5.47 GHz mainly attributes to the effect of the band-notched structure. Similar performance is observed for Ant-3, as shown in Figure 8(b).

3. EQUIVALENT CIRCUITS ANALYSIS AND PARAMETRIC STUDIES

In order to further explain the principle of the segmented structure and how the notch frequencies and bandwidths can be controlled, we make equivalent lumped circuit analysis in this section. Generally, the input impedance of an UWB PMA can be represented by the first Foster canonical form [19]. In other words, matched bandwidth of UWB PMA can be considered as the result of several adjacent resonance modes. Each mode can be represented by a parallel RLC resonator [16, 20]. For band-notched UWB PMAs, the bandstop function is achieved by introducing a coupling resonance structure that can be represented by an additional RLC resonator.

Figure 9 shows the HFSS simulated input impedance of Ant-1.

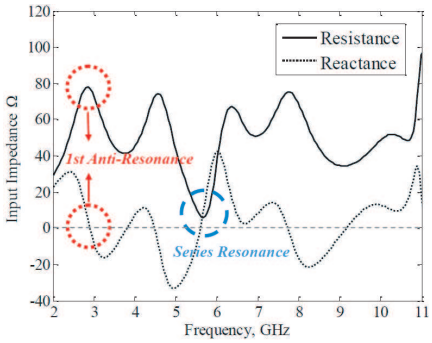

Figure 9. HFSS simulated input impedance of Ant-1.

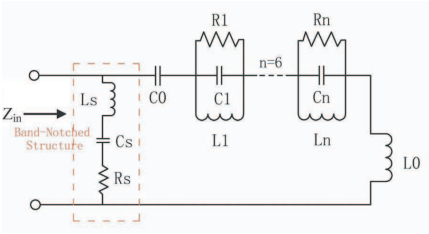

Figure 10. Equivalent lumped circuit model for Ant-1.

According to the figure, six obvious anti-resonance modes are observed in the solution band (2 GHz $\sim$ 11 GHz). However, at the notch frequency 5.7 GHz, input impedance is quite similar to the impedance of a series RLC circuit, i.e., the imaginary part is nearly crossing zero and has a positive derivative, while the real part has a local minimum (5.8 Ω). The impedance is nearly zero at the feeding point, which leads to the desired impedance mismatch at that frequency. In this case, the equivalent circuit model of Ant-1 is proposed, as shown in Figure 10. Input impedance in the passband is represented by six parallel RLC cells in series, whereas a shunt RLC-in-series resonator denotes the contribution of the band-notched structure. The equivalent circuit input impedance can be expressed as formulas (1)–(4)

$$Z_{in}(\omega) = \frac{Z_a(\omega)Z_s(\omega)}{Z_a(\omega) + Z_s(\omega)} \tag{1}$$

$$Z_s(\omega) = R_s\left[1 + jQ_s\left(\frac{\omega}{\omega_s} - \frac{\omega_s}{\omega}\right)\right] \tag{2}$$

$$Q_s = \frac{1}{R_s}\sqrt{\frac{L_s}{C_s}} = \frac{1}{R_s C_s \omega_s} \tag{3}$$

$$Z_a(\omega) = j\left(\omega L_0 - \frac{1}{\omega C_0}\right) + \sum_{i=1}^{n} \frac{R_i}{1 + jQ_i\left(\frac{\omega}{\omega_i} - \frac{\omega_i}{\omega}\right)} \tag{4}$$

where $\omega_i = \frac{1}{\sqrt{L_i C_i}}$ and $Q_i = R_i\sqrt{\frac{C_i}{L_i}} = R_i C_i \omega_i$ represent the resonant angular frequency and the quality factor of each parallel RLC cell, respectively.

Sufficient impedance data can be obtained from the HFSS

Table 1. Element values of the equivalent circuit model for Ant-1.

C_0 (pF)	*Band-notched Resonator*		*RLC Cells*	**1**	**2**	**3**	**4**	**5**	**6**
2.19	R_s (Ω)	6	R_i (Ω)	68	53	51	46	35	53
L_0 (nH)	Q_s	63	Q_i	2.3	4.5	4.3	5.6	6	24
0.59	f_s (GHz)	5.645	f_i (GHz)	2.88	4.75	5.78	7.65	10.2	11

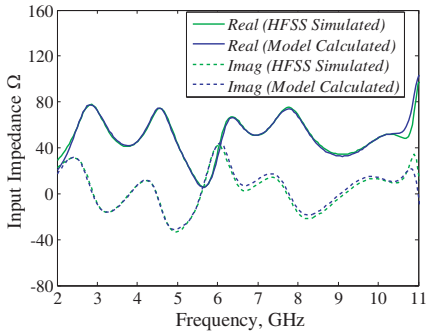

Figure 11. Comparison between the input impedance of Ant-1 simulated by HFSS and by the equivalent circuit model in Figure 10.

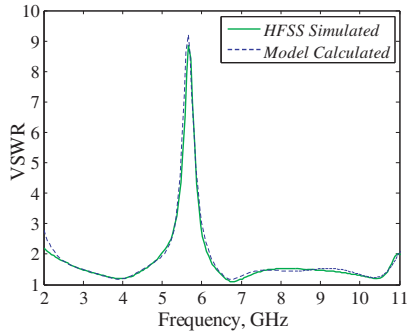

Figure 12. Comparison between the VSWR of Ant-1 simulated by HFSS and by the equivalent circuit model in Figure 10.

simulated results. With these data and various data-fitting approaches [20], the values of the unknown parameters in (2)–(4) are determined, which are listed in Table 1. Figure 11 compares the Ant-1 input impedance simulated by HFSS to that calculated by the equivalent circuit model. Figure 12 shows the comparison between the VSWR values of Ant-1 simulated by HFSS and calculated by the proposed model. It is observed that the output of the proposed model is nearly indistinguishable with the fullwave simulation results. Note that, this model is suitable for band-notched UWB planar monopole antennas which exhibit short-circuit-like input impedance at the notch frequency, such as Ant-1 and Ant-3 presented in this paper.

Figure 13 shows the HFSS simulated input impedance of Ant-2. At the notch frequency 5.56 GHz, the reactance is nearly crossing zero and has a negative derivative, whereas the resistance has a local

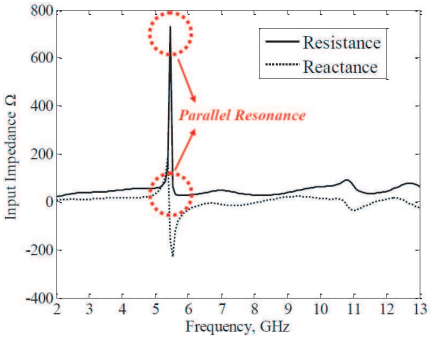

Figure 13. HFSS simulated input impedance of Ant-2.

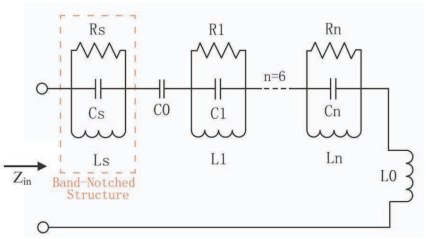

Figure 14. Equivalent lumped circuit model for Ant-2.

maximum. It is a typical parallel-type resonance (anti-resonance) with large and rapid changes in the values of the impedance, both the real and the imaginary parts. In this case, corresponding equivalent circuit model is proposed, as shown in Figure 14, where an additional parallel RLC resonator (R_s, C_s and L_s) is incorporated to represent the band-notched structure. The input impedance of the model is expressed as

$$Z_a(\omega) = \frac{R_s}{1 + jQ_s\left(\frac{\omega}{\omega_s} - \frac{\omega_s}{\omega}\right)} + j\left(\omega L_0 - \frac{1}{\omega C_0}\right) + \sum_{i=1}^{n} \frac{R_i}{1 + jQ_i\left(\frac{\omega}{\omega_i} - \frac{\omega_i}{\omega}\right)} \quad (5)$$

All the unknown parameters in (5) are obtained using data fitting approach, and are shown in Table 2. Figure 15 compares the Ant-2 input impedance simulated by HFSS to that calculated by the equivalent circuit model. Figure 16 shows the comparison between the VSWR values of Ant-2 simulated by HFSS and calculated by the proposed model. Very good agreement in port characteristics is achieved. This model is suitable for band-notched UWB planar monopole antennas which exhibit open-circuit-like input impedance at the notch frequency.

On the basis of the above equivalent circuit analysis, we have a clear method for controlling the notch frequency and the bandwidth of the notched band. The current propagating along the edges of the slots is equivalent to the inductor L_s, while the narrow slot is equivalent to the capacitor C_s. By adjusting the inductor and capacitor values, suitable notch frequency and bandwidth can be achieved. In these designs, the key parameters that impact the band-notched functions are the distance between the slots $2 \times Ds$ and the width of the slots Ws

Table 2. Element values of the equivalent circuit model for Ant-2.

C_0 (pF)	*Band-notched Resonator*		*RLC Cells*	**1**	**2**	**3**	**4**	**5**	**6**
1.62	R_s (Ω)	772	R_i (Ω)	20	50	21	48	45	63
L_0 (nH)	Q_s	101	Q_i	2.2	1.3	7	5	24	11
0.55	f_s (GHz)	5.540	f_i (GHz)	2.88	4.69	7.05	10.1	10.8	12.7

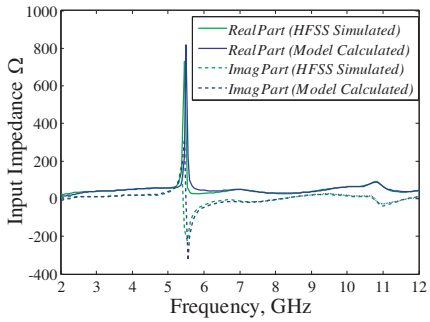

Figure 15. Comparison between the input impedance of Ant-2 simulated by HFSS and by the equivalent circuit model in Figure 14.

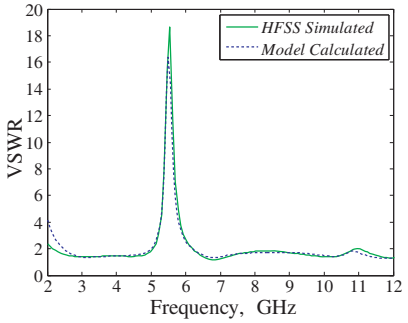

Figure 16. Comparison between the VSWR of Ant-2 simulated by HFSS and by the equivalent circuit model in Figure 14.

Figure 17 shows the simulated VSWR of Ant-1 for different *Ds* that denotes the position of the segmenting slots. As shown in the figure, when the slots move away from each other (*Ds* increasing), the length of the slots decrease, which is similar to decreasing the capacitor value C_s and the inductor value L_s. As a result, the notch frequency increases. It is worth mentioning that spurious stop bands are introduced by the high-order harmonics of the segmented structure. The high-order resonant frequencies also increase as *Ds* increases. Moreover, it is observed that as *Ds* increases, the VSWR values at the notch frequency and high-order resonant frequencies are greatly reduced. This is probably owing to the fact that the coupling effect around the segmented structure gets weak as the segmenting slots move away from the feeding point. Considering the influence of the spurious harmonics of the segmented structure, a compromise should be made

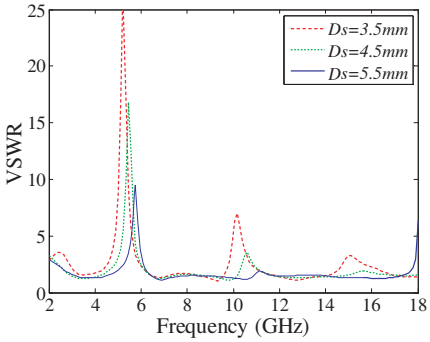

Figure 17. Simulated VSWR for Ant-1 in terms of *Ds*.

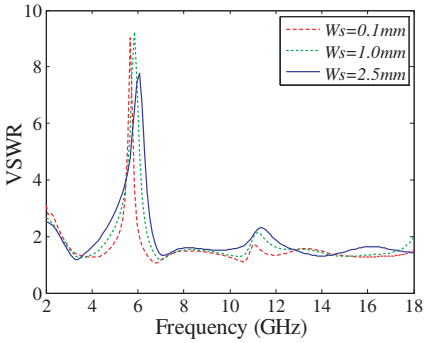

Figure 18. Simulated VSWR for Ant-1 in terms of *Ws*.

between the maximum VSWR and the passband bandwidth. The simulations indicate the best band-notched property achieved when the distance between the vertical slots is around the half of the patch width.

On the other hand, the notch bandwidth mainly depends on the quality factor Q_s of the band-notched structure. Figure 18 exhibits the effect of *Ws* on the notch bandwidth of Ant-1. It is observed that the increasing of *Ws* weakens the coupling among the central patch and the side patches. This produces a decreasing in both electric field and surface current around the segmenting slots. Therefore, both L_s and C_s decline as *Ws* increases, but L_s declines faster than C_s, so their ratio (L_s/C_s) globally decreases. As a result, the quality factor Q_s of the band-notched structure reduces, and consequently the notch bandwidth is broadened.

Similarly, the notch frequencies and bandwidths of Ant-2 and Ant-3 can also be controlled by tuning corresponding parameters *Ds* and *Ws*. For simplicity, these results are not depicted.

4. CONCLUSION

A new segmented structure is proposed as a versatile method to achieve band-notched function for UWB PMAs. The design methodology is simple by segmenting the monopole patch into three parts. To verify the effectiveness of the segmented approach, three PMAs with commonly used patch shapes of circle, beveled rectangle and regular hexagon are carefully selected and investigated. Good agreement is achieved between the measurements and the simulations. The measured results show that band-notched performance from 5–6 GHz

is obtained for each of the antennas by utilizing our approach. Furthermore, a pair of equivalent lumped circuit models based on the analysis of resonance phenomena has been proposed and verified. According to these models, the center frequency and bandwidth of the notched band can be adjusted within a certain range by optimizing a few key parameters. Generally, the segmented structure could be regarded as a hybrid between the methods of cutting slots and attaching parasitic elements. But it is more straightforward because the parasitic elements (side patches) are generated automatically by segmenting the patch. It also has a simpler optimization owing to the lower number of degrees of freedom in the cuts. It is reasonable to deduce that the proposed structure would probably be appropriated for other UWB PMAs with patch shapes of ellipse, semicircle, triangle and other polygons.

REFERENCES

1. Lin, C. C. and H. R. Chuang, "A 3–12 GHz UWB planar triangular monopole antenna with ridged ground-plane," *Progress In Electromagnetics Research*, Vol. 83, 307–321, 2008.
2. Zaker, R., C. Ghobadi, and J. Nourinia, "A modified microstrip-fed two-step tapered monopole antenna for UWB and WLAN applications," *Progress In Electromagnetics Research*, Vol. 77, 137–148, 2007.
3. Liang, J. X., C. C. Chiau, X. D. Chen, and C. G. Parini, "Study of a printed circular disc monopole antenna for UWB systems," *IEEE Trans. on Ntennas and Propag.*, Vol. 53, 3500–3504, 2005.
4. Chen, Z. N., T. S. P. See, and X. M. Qing, "Small printed ultrawideband antenna with reduced ground plane effect," *IEEE Trans. on Antennas and Propag.*, Vol. 55, 383–388, 2007
5. Barbarino, S. and F. Consoli, "UWB circular slot antenna provided with an inverted-L notch filter for the 5 GHz WLAN band," *Progress In Electromagnetics Research*, Vol. 104, 1–13, 2010.
6. Chu, Q. X. and Y. Y. Yang, "A compact ultrawideband antenna with 3.4/5.5 GHz dual band-notched characteristics," *IEEE Trans. on Antennas and Propag.*, Vol. 56, 3637–3644, 2008.
7. Li, C.-M. and L.-H. Ye, "Improved dual band-notched UWB slot antenna with controllable notched band-widths," *Progress In Electromagnetics Research*, Vol. 115, 477–493, 2011.
8. Qu, S., J. Li, and Q. Xue, "A band-notched ultrawideband

printed monopole antenna," *IEEE Antennas Wireless Propag. Lett.*, Vol. 5, 495–498, 2006.

9. Sim, C.-Y.-D., W.-T. Chung, and C.-H. Lee, "Planar UWB antenna with 5 GHz band rejection switching function at ground plane," *Progress In Electromagnetics Research*, Vol. 106, 321–333, 2010.
10. Jiang, J., Y. Song, Z. Yan, X. Zhang, and W. Wu, "Band-notched UWB printed antenna with an inverted-L-slotted ground," *Microwave. Opt. Technol. Lett.*, Vol. 51, 260–263, 2009.
11. Kelly, J. R., P. S. Hall, and P. Gardner, "Band-notched UWB antenna incorporating a microstrip open-loop resonator," *IEEE Trans. on Antennas and Propag.*, Vol. 59, 3045–3048, 2011.
12. Thomas, K. G. and M. Sreenivasan, "A simple ultrawideband planar rectangular printed antenna with band dispensation," *IEEE Trans. on Antennas and Propag.*, Vol. 58, 27–34, 2010.
13. Abbosh, A. M. and M. E. Bialkowski, "Design of UWB planar band-notched antennas using parasitic elements," *IEEE Trans. on Antennas and Propag.*, Vol. 57, 796–799, 2009.
14. Peng, L. and C. L. Ruan, "UWB band-notched monopole antenna design using electromagnetic-bandgap structures," *IEEE Trans. on Microwave Theory and Tech.*, Vol. 59, 1074–1081, 2011.
15. Lin, C. C., P. Jin, and W. Ziolkowski, "Single, dual and tri-band-notched ultrawideband (UWB) antennas using Capacitively loaded loop (CLL) resonators," *IEEE Trans. on Antennas and Propag.*, Vol. 60, 102–109, 2012.
16. Wang, S. B. T., A. M. Niknejad, and W. Brodersen, "Circuit modeling methodology for UWB omnidirectional small antennas," *IEEE J. Select. Areas Commun.*, Vol. 24, 871–877, 2006.
17. Zhang, K., Y. X. Li, and Y. L. Long, "Band-notched UWB printed monopole antenna with a novel segmented circular patch," *IEEE Antennas Wireless Propag. Lett.*, Vol. 9, 1209–1212, 2010.
18. Collin, R. E., *Foundation for Microwave Engineering*, 2nd Edition, McGraw-Hill, New York, 1993.
19. Ramo, S., J. R. Whinnery, and T. Van Duzer, *Fields and Waves in Communication Electronics*, Wiley, New York, 1994.
20. Pele, I., A. Chousseaud, and S. Toutain, "Simultaneous modeling of impedance and radiation pattern antenna for UWB pulse modulation," *IEEE APS Int. Symp. Dig.*, Vol. 2, 1871–1874, Monterey, CA, Jun. 2004.